JOURNAL OF COMPUTATIONAL PHYSICS **140,** 346–369 (1998)
ARTICLE NO. CP985897

An Efficient Algorithm for Truncating Spatial Domain in Modeling Light Scattering by Finite-Difference Technique

Ping Yang and K. N. Liou

Department of Atmospheric Sciences, University of California at Los Angeles, Los Angeles, California 90095
E-mail: yang@climate.met.utah.edu, knliou@atmos.ucla.edu

Received December 18, 1996; revised November 24, 1997

The finite-difference time domain technique is one of the most robust and accurate numerical methods for the solution of light scattering by small particles with arbitrary composition and geometry. In practice, this method requires that the spatial domain for the computation of near-field be truncated. An absorbing boundary condition must be imposed in conjunction with this truncation. The performance of this boundary condition is essential to the stability of numerical computations and the reliability of results. In the present study, a new boundary condition, referred to as the mixed T algorithm, has been developed, which is a generalization of the transmitting boundary condition originally developed by Liao and co-workers. The present algorithm does not require spatial interpolation for wave values at interior grid points. In addition, it produces two minima of spurious reflections at small and large incident angles, allowing efficient absorption of the scattered waves at the boundary for large incident angles. When the third-order mixed T algorithm is used, the reflection coefficient of the boundary is less than 1% for incident angles from 0° to about 70°. We find that the numerical instability associated with the transmitting boundary condition is caused by the location-dependent amplitude of outgoing waves in the vicinity of the boundary. For this reason, the mixed T algorithm is stabilized by consistently introducing diffusive coefficients into the boundary equation. When the stabilized algorithm is applied, the near-field within the truncated domain can be computed by using single-precision arithmetic without overflows for more than 10^5 steps in the time-marching iteration. Finally, the new absorbing boundary condition is validated by carrying out numerical experiments involving the propagation of a TM wave excited by a sinusoidal point source, simultaneous simulation of the wave propagation in small and large domains, and the scattering of a TM wave by an infinite circular cylinder.

Key Words: boundary condition; computational domain; finite-difference; light scattering.

0021-9991/98 $25.00

1. INTRODUCTION

Solution of light scattering by nonspherical particles is of fundamental interest in many disciplines including atmospheric remote sensing and radiative transfer [1, 2]. Most of the naturally occurring particles such as ice crystals and nonspherical aerosols in the atmosphere cannot be approximated as spheres or spheroids with acceptable accuracy [3]. It is unlikely that the scattering properties of these nonspherical particles can be solved analytically because proper coordinate systems cannot be defined to impose the electromagnetic boundary condition on the particle surface. The inhomogeneous composition of the scattering particles will further complicate the solution. For this reason, numerical approaches must be applied to compute the scattering properties of nonspherical particles. It has been recognized that the finite-difference time domain (FDTD) technique pioneered by Yee [4] is a powerful numerical approach to solve the electromagnetic scattering problem concerning an object of arbitrary shape and inhomogeneous composition [5–7]. In practice, the FDTD method is applicable only to the computation of near-field within a finite spatial region because the panorama of the time-dependent field in unbounded space cannot be handled by any computational resource. Transformation from near-field to far-field is also required for practical applications. Thus, an artificial boundary must be used to truncate the infinite region within which the scattering process takes place. To ensure the simulated field within the truncated domain is the same as in the unbounded case, the artificial boundary must have a condition known as absorbing or transmitting boundary condition (ABC or TBC). Otherwise, the spurious reflections from the boundary can contaminate the near-field within the truncated domain.

The development of ABC has been a subject of active research until now, because the performance of the boundary condition is critical to the accuracy of numerical simulations. In addition, the "white space" between the boundary and scatterer, required by a specific boundary condition, is an important factor determining the computational cost. The earliest implementation of ABC in conjunction with the application of the FDTD technique to electromagnetic scattering problems was the average space-time extrapolating method [5], although the implementation of ABC can trace back to the solution of the hydrodynamic problems based on the Sommerfeld radiation condition [8]; see, e.g., Vastono and Reid [9]. Other approaches, such as the mode-annihilating operator [10] and the extrapolating scheme based on the Poynting vector of the scattered wave [11], have also been developed to suppress the reflection of the artificial boundary. However, the ABCs derived from the one-way wave equation (OWWE) appear to have been extensively studied. As reviewed by Moore *et al.* [12] and Blaschak and Kriegsmann [13], various kinds of approximations of the pseudo-differential operator in OWWE have been developed. Among them, the algorithm developed by Mur [14] (hereafter referred to as Mur's ABC) has been widely used in the implementation of the FDTD technique. The second or higher order Mur's ABC involves the wave values at the intersections of boundary faces. However, the corresponding boundary equations cannot be posed in self-closing form; that is, a less accurate first-order formula or an extrapolating scheme must be used at the intersections. Moreover, Mur's algorithm is rather tedious, especially in the higher order formulation in the three-dimensional (3D) case. In the computation of the scattering of electromagnetic waves by the FDTD method, the field values at the intersections are not required for updating the field values at interior grid points. Thus, it is desirable to construct an ABC that can circumvent the disadvantage associated with the requirement of field values at the intersections. We find that the TBC

developed by Liao *et al.* [15] (hereafter referred to as Liao's TBC) is a good approach for the solution of a light scattering problem based on FDTD.

Liao's TBC is based on the principle of wave propagation; that is, wave values at the boundary are the arrivals of wave disturbances at certain interior points. A completely reflectionless ABC can be constructed for normal incidence or the one-dimensional (1D) case, as noted by Taflove and Brodwin [5]. However, in the two-dimensional (2D) or the 3D case with oblique incidence, the interior points cannot be located due to the unknown incident angle of outgoing waves. To overcome this difficulty, Liao *et al.* [15] developed the multitransmitting method to define the boundary values in terms of the interior values equally spaced along the directions normal to the boundary faces. However, the interior points, in practice, may not be consistent with the computational grid points; thus, an interpolation of wave values is required. In addition, Liao's TBC requires double-precision arithmetic in numerical computation to achieve stability. This increases the computational cost by two to three times. Significant reflections are also found for this boundary condition at large incident angles. For these reasons, we have developed a more economic, stable, and accurate boundary condition in conjunction with the application of the FDTD method to the solutions of light scattering by nonspherical particles.

2. IMPROVED TRANSMITTING BOUNDARY CONDITION

A. *Conceptual Basis of Transmitting Boundary Condition*

In the methodology associated with the implementation of ABCs or TBCs to an outgoing or scattered wave, it is assumed that the outgoing scattered wave can be approximated as a plane wave (not necessarily a time-harmonic plane wave) in the vicinity of the boundary locally. Under such an assumption, the multitransmitting theory [15] can be used to construct a transparent or reflectionless boundary. In this subsection we outline, without the mathematical details, the conceptual basis for the TBC developed by Liao *et al.* [15] and discuss its shortcomings in numerical computations.

Liao *et al.* [15] postulated that the original outgoing wave can be transmitted through the boundary along the direction normal to the boundary face in an artificial transmitting speed, leading to a remained error wave. This error wave can also be transmitted in the same manner. Consequently, a second-order error wave is produced. After this procedure is carried out sequentially, the outgoing wave can be transmitted through the boundary eventually regardless of incident angle. Based on this principle, the wave values at a boundary, say, the right side boundary ($x = x_b$), can be expressed as

$$U(t + \Delta t, x_b) = \sum_{L=1}^{N} (-1)^{L+1} \frac{N!}{(N-L)!L!} U[t - (L-1)\Delta t, x_b - Lc_\alpha \Delta t], \qquad (2.1)$$

where U is the wave value, c_α is an artificial transmitting speed which may differ from that of the corresponding real physical wave, and Δt is the temporal increment used in the discrete calculation. Since the ratio of the temporal increment to the spatial increment in the finite computation is subject to the Courant–Friedrichs–Levy (CFL) condition [5] for numerical stability, the wave values on the right-hand side of (2.1) are usually not located at grid points. To circumvent the shortcoming, Liao *et al.*[15] used a quadratic interpolation

to obtain the wave values and developed the algorithm

$$U(t+\Delta t, x_b) = \sum_{L=1}^{N} (-1)^{L+1} \frac{N!}{(N-L)!L!} \overline{T}^L \overline{U}_L, \tag{2.2a}$$

$$\overline{T}^L = [T_{L,1}, T_{L,2}, \ldots, T_{L,2L+1}], \tag{2.2b}$$

$$\overline{U}_L = [U_{1,L}, U_{2,L}, \ldots, U_{2L+1,L}]^T, \tag{2.2c}$$

where the superscript T denotes the transpose of the matrix, and $U_{i,j} = U[t-(j-1)\Delta t, x_b - (i-1)\Delta s]$ in which Δs is the spatial increment of the numerical grid. The matrix $\overline{T}^L$ can be calculated from

$$\overline{T}^L = \overline{T}^1 \begin{bmatrix} T_{L-1,1} & T_{L-1,2} & \cdots & \cdots & T_{L-1,2L-1} & 0 & 0 \\ 0 & T_{L-1,1} & T_{L-1,2} & \cdots & \cdots & T_{L-1,2L-1} & 0 \\ 0 & 0 & T_{L-1,1} & T_{L-1,2} & \cdots & \cdots & T_{L-1,2L-1} \end{bmatrix} \quad \text{for } L \geq 2, \tag{2.2d}$$

in which the three elements of $\overline{T}^1$ are $T_{1,1} = (2-\beta)(1-\beta)/2$, $T_{1,2} = \beta(2-\beta)$, and $T_{1,3} = \beta(\beta-1)/2$, where $\beta = c_\alpha \Delta t/\Delta s$. It is noted that interpolations will reduce the computational efficiency.

Moghaddam and Chew [16] have pointed out that to stabilize the algorithm given by (2.2) double-precision arithmetic must be used in numerical computations. More recently, Chew and Wagner [17] also found that significant spurious reflections can be caused by the preceding algorithm for large incident angles. They further noted that the performance of the TBC could be greatly improved by using various artificial transmitting speeds in the interpolation of the wave values simultaneously.

B. *Transmitting Boundary Condition Derived from Optimized Extrapolation*

In the construction of the transmitting boundary condition, Liao *et al.* [15] assumed that the transmission of the outgoing wave consists of the original wave and various orders of error waves. Such an explanation is somewhat misleading because fictitious waves, which may propagate faster than real physical waves, are implied. We find that TBC is essentially an extrapolating scheme to determine the boundary values in terms of optimal extrapolation coefficients. Therefore, without introducing the concept of error waves and the ad hoc artificial transmitting speed, we derive an analog of TBC, in which the involved interior values are located only at grid points, avoiding the interpolation of wave values at interior points. As shown in Fig. 1, an outgoing or scattered wave strikes the boundary at incident angle α. Since the wave can be approximated as a plane wave in the vicinity of the boundary locally, it can be expressed in the OX system as

$$U(t, x) = U(ct - x\cos\alpha). \tag{2.3}$$

From (2.3), the wave value at the boundary of $x = x_b$ can be written in the form

$$\begin{aligned} U(t, x_b) &= U(ct - x_b \cos\alpha) \\ &= U[c(t - L\Delta s \cos\alpha/c) - (x_b - L\Delta s)\cos\alpha] \\ &= U(t - L\Delta s \cos\alpha/c, x_b - L\Delta s), \end{aligned} \tag{2.4}$$

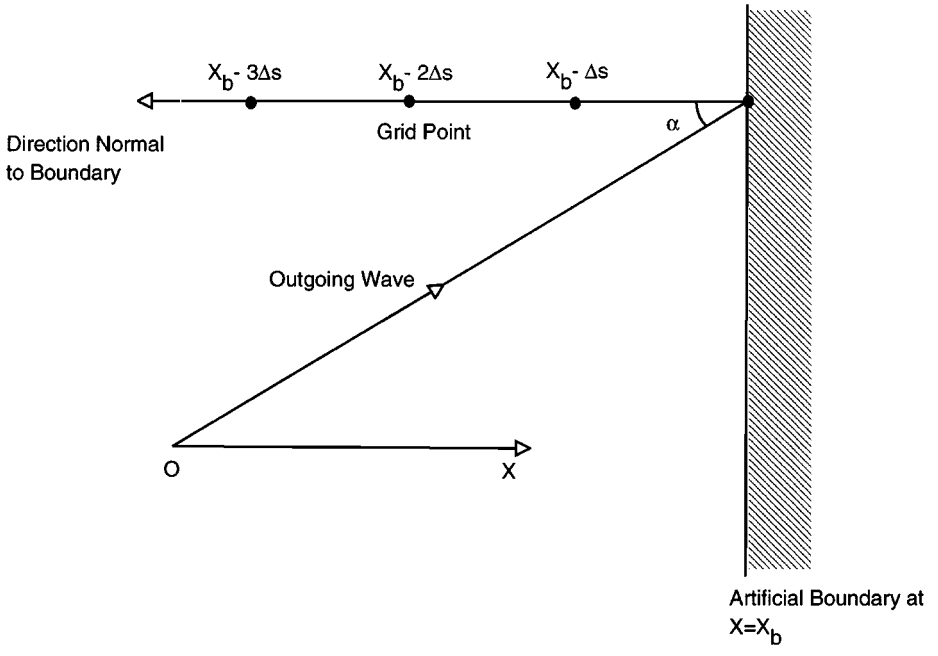

FIG. 1. Geometry for an outgoing or scattered wave in the vicinity of an artificial boundary.

where L is an arbitrarily selected integer and $(x_b - L\Delta s)$ (L = 1, 2, 3, . . .) are the locations of the interior grid points. Equation (2.4) indicates that the boundary values at time = t is the arrival of the interior values located at $x_b - L\Delta s$ at time $= t - L\Delta s \cos\alpha / c$. However, since the incident angle α is unknown in practice, (2.4) is not useful in numerical computations. To circumvent the uncertainty caused by the unknown incident angle, we define the quantity

$$d_L = U(t - L\Delta s \cos\alpha/c, x_b - L\Delta s) - U(t - L\Delta\tilde{t}, x_b - L\Delta s), \quad L = 1, 2, 3, \ldots, \tag{2.5}$$

where $\Delta\tilde{t}$ is a small increment in time, which may differ from the temporal increment Δt used in the finite difference computation. Then, from (2.4) and (2.5) we can obtain an exact relationship given by

$$U(t, x_b) = \sum_{L=1}^{N} g_L U(t - L\Delta\tilde{t}, x_b - L\Delta s) + \sum_{L=1}^{N} g_L d_L, \tag{2.6a}$$

$$\sum_{L=1}^{N} g_L = 1, \tag{2.6b}$$

where $\{g_L, L = 1, 2, 3, \ldots\}$ is a set of constant coefficients. Although the second term on the right-hand side of (2.6a) is unknown, we can minimize this term by properly specifying g_L. Applying the Taylor expansion to (2.5) along with the plane wave condition given in (2.3), we obtain

$$d_L = \sum_{m=1}^{\infty} \frac{1}{m!} \frac{d^{(m)}U(\eta)}{d\eta^m}\bigg|_{\eta=\xi} L^m \xi^m, \tag{2.7a}$$

$$\xi = \Delta s \cos\alpha - c\Delta\tilde{t}, \tag{2.7b}$$

which are followed by

$$\sum_{L=1}^{N} g_L d_L = \sum_{m=1}^{\infty} \left[\frac{1}{m!} \frac{d^{(m)}U(\eta)}{d\eta^m}\bigg|_{\eta=\xi} \xi^m \left(\sum_{L=1}^{N} g_L L^m \right) \right]. \tag{2.8}$$

Therefore, the optimal selection of $\{g_L, L = 1, 2, 3, \ldots, N\}$ should satisfy (2.6b) and $\sum_{L=1}^{N} g_L L^m = 0$ for $m = 1, 2, 3, \ldots, N-1$; that is,

$$\begin{bmatrix} 1 & 1 & 1 & \ldots & \ldots & 1 & 1 \\ 1 & 2 & 3 & \ldots & \ldots & N-1 & N \\ 1 & 2^2 & 3^2 & \ldots & \ldots & (N-1)^2 & N^2 \\ \ldots & \ldots & \ldots & \ldots & \ldots & \ldots & \ldots \\ 1 & 2^{N-2} & 3^{N-2} & \ldots & \ldots & (N-1)^{N-2} & N^{N-2} \\ 1 & 2^{N-1} & 3^{N-1} & \ldots & \ldots & (N-1)^{N-1} & N^{N-1} \end{bmatrix} \begin{bmatrix} g_1 \\ g_2 \\ g_3 \\ \vdots \\ g_{N-1} \\ g_N \end{bmatrix} = \begin{bmatrix} 1 \\ 0 \\ 0 \\ \vdots \\ 0 \\ 0 \end{bmatrix}. \tag{2.9}$$

The determinant of the coefficient matrix of the preceding equation is a special form of the well-known van der Monde determinant. According to the Cramer rule, the solution for (2.9) is given by

$$g_L = (-1)^{L+1} \frac{N!}{(N-L)!L!}, \quad L = 1, 2, 3, \ldots, N. \tag{2.10}$$

Further, it can be proven that

$$\frac{1}{N!} \sum_{L=1}^{N} (-1)^{L+1} \frac{N!}{(N-L)!L!} L^N = (-1)^{N+1}. \tag{2.11}$$

With the coefficients $\{g_L, L = 1, 2, 3, \ldots\}$ defined by (2.10), the truncation error denoted in (2.8) is insignificant. To evaluate the magnitude of the truncation error, let us consider a harmonic plane wave mode defined by

$$U(t, x) = U(ct - x\cos\alpha) = e^{-ik(ct - x\cos\alpha)}. \tag{2.12}$$

It follows that

$$\left| \frac{d^{(m)}U(\eta)}{d\eta^m}\bigg|_{\eta=\xi} \xi^m \right| = |(-ik)^m e^{-ik\xi} \xi^m| \le |k_{max}\xi|^m, \tag{2.13}$$

where $k_{max} = 2\pi/\lambda_{min}$ in which λ_{min} is the minimum wavelength allowed by the numerical grid. To circumvent the numerical dispersion occurring in the finite-difference approximations, we usually select $\Delta s/\lambda_{min} \le 20$ in numerical computation. Furthermore, as will be seen in the following discussion, $(\cos\alpha - c\Delta\tilde{t}/\Delta s)$ is less than unity. Thus, we have

$$|k_{max}\xi|^m = \left| \frac{2\pi}{\lambda_{min}} \Delta s(\cos\alpha - c\Delta\tilde{t}/\Delta s) \right|^m \ll 1 \quad \text{for } m > 1 \tag{2.14}$$

and we obtain

$$\sum_{L=1}^{N} g_L d_L = (-1)^{N+1} \frac{d^{(N)}U(\eta)}{d\eta^N}\bigg|_{\eta=\xi} \xi^N + \sum_{m=N+1}^{\infty} \left[\frac{1}{m!} \frac{d^{(m)}U(\eta)}{d\eta^m}\bigg|_{\eta=\xi} \xi^N \sum_{L=1}^{N} L^m \frac{N!}{(N-L)!L!} \right]$$

$$\approx O\left[\frac{d^{(N)}U(\eta)}{d\eta^N}\bigg|_{\eta=\xi} \xi^N \right] \approx O[(k_{max}\xi)^N]. \tag{2.15}$$

An approximate expression for the boundary condition can subsequently be obtained from (2.6a) and (2.15) in the form

$$U(t, x_b) = \sum_{L=1}^{N} (-1)^{L+1} \frac{N!}{(N-L)!L!} U(t - L\Delta\tilde{t}, x_b - L\Delta s) + O[(k_{max}\xi)^N]. \tag{2.16}$$

Comparing (2.1) with (2.16), we note that they are equivalent, provided that $\Delta\tilde{t} = \Delta t$ and $c_\alpha \Delta\tilde{t} = \Delta s$. It is evident that all the wave values involved in (2.16) are located at grid points. Accordingly, the interpolation required by Liao's algorithm can be avoided by using the present boundary condition. It is also evident from (2.15) and (2.16) that the boundary condition is completely reflectionless if $\xi = 0$; that is

$$\Delta s \cos\alpha - c\Delta\tilde{t} = 0, \quad \text{or} \quad \cos\alpha = c\Delta\tilde{t}/\Delta s. \tag{2.17}$$

In the implementation of FDTD, $\Delta t = \Delta s/2$ is usually selected for a sufficient stability requirement, which is very close to the maximum temporal increment allowed by the CFL condition in the 3D case [5]. Therefore, if we select $\Delta\tilde{t} = \Delta t$, then the boundary is reflectionless at incident angle of 60°. On the other hand, the incident angle corresponding to the complete transmission is 0° if we select $\Delta\tilde{t} = 2\Delta t$.

C. *Mixed T Algorithm*

The performance of an absorbing boundary condition is generally characterized by the reflection coefficient associated with it. We shall express (2.16) in a concise operator form to study the reflecting characteristics of the boundary condition. Following Chew and Wagner [17], we define the space-shifting operator $G(\Delta s)$ and time-advancing operator $T(\Delta\tilde{t})$ as

$$G(\Delta s)U(t, x_b) = U(t, x_b - \Delta s), \tag{2.18a}$$

$$T(\Delta\tilde{t})U(t, x_b) = U(t - \Delta\tilde{t}, x_b). \tag{2.18b}$$

According to the definitions of these operators and the binomial formula, we can rewrite (2.16) in the form

$$[1 - T(\Delta\tilde{t})G(\Delta s)]^N U(t, x_b) = 0. \tag{2.19}$$

In numerical computations, the second or third order formula of the boundary condition is generally used. If we select $T(\Delta\tilde{t}) = T(\Delta t)$ (hereafter referred to as the T algorithm), then

the third-order formula in finite difference form is given by

$$U^{n+1}(I_b, J, K) = 3U^n(I_b - 1, J, K) - 3U^{n-1}(I_b - 2, J, K) + U^{n-2}(I_b - 3, J, K), \quad (2.20)$$

where the indices I, J, and K denote $(x, y, x) = (I, J, K)\Delta s$, I_b denotes the right-side boundary, and n is the time step. On the other hand, if we select $T(\Delta\tilde{t}) = T(2\Delta t) = T^2(\Delta t)$ (hereafter referred to as the T^2 algorithm), then the third-order algorithm is given by

$$U^{n+1}(I_b, J, K) = 3U^{n-1}(I_b - 1, J, K) - 3U^{n-3}(I_b - 2, J, K) + U^{n-5}(I_b - 3, J, K). \quad (2.21)$$

Equations (2.20) and (2.21) are for the 3D case. It should be noted that the boundary equations are in the same form for both the 2D and the 3D cases. We have applied the third-order T^2 algorithm to solve the scattering of light by ice crystals in our previous study in which the instability of the algorithm has been removed by weighing the third-order boundary equation with its second-order counterpart [18].

Although the T and T^2 algorithms are given by similar expressions, as shown in (2.20) and (2.21), their reflecting features are significantly different. Let us consider a harmonic plane wave impinging on the right boundary. After the incident wave interacts with the boundary, the total wave in the proximity of the boundary can be expressed as

$$U^n(I, J, K) = e^{i(k_y J\Delta s + k_z K\Delta s - \omega n\Delta t)} e^{ik_x I\Delta s} + Re^{i(k_y J\Delta s + k_z K\Delta s - \omega n\Delta t)} e^{-ik_x I\Delta s}, \quad (2.22)$$

where the first and second terms on the right-hand side stand for the incident and reflected waves, respectively, and R is the reflection coefficient of the boundary. Substituting (2.22) into (2.20) and (2.21), we obtain the reflection coefficients, R_T and R_{T^2}, for the T and T^2 algorithms, respectively, as

$$R_T = -e^{i2k_x\Delta s I_b} e^{-i3k_x\Delta s} \left\{ \frac{\sin[k\Delta s(c\Delta t/\Delta s - \cos\alpha)/2]}{\sin[k\Delta s(c\Delta t/\Delta s + \cos\alpha)/2]} \right\}^3, \quad (2.23a)$$

$$R_{T^2} = -e^{i2k_x\Delta s I_b} e^{-i3k_x\Delta s} \left\{ \frac{\sin[k\Delta s(2c\Delta t/\Delta s - \cos\alpha)/2]}{\sin[k\Delta s(2c\Delta t/\Delta s + \cos\alpha)/2]} \right\}^3. \quad (2.23b)$$

The magnitude of the reflection coefficients is shown in Fig. 2. It is clear that the T^2 algorithm performs quite well for the incident angles smaller that 30°, but we note that the reflection significantly increases when the angle is larger than 45°. The performance of the T algorithm, however, is much improved for large incident angles. The accuracy of the boundary condition can be significantly improved if the advantages of the preceding two algorithms are combined. To accomplish this, we rewrite (2.19) as

$$[1 - T(\Delta t)G(\Delta s)]^{N-M}[1 - T^2(\Delta t)G(\Delta s)]^M U(t, x_b) = 0, \quad (2.24)$$

where the integer M should be smaller than N. Since the time-advancing operators involved in (2.24) are from both the T and T^2 algorithms, the algorithm given by (2.24) will be referred to as the mixed T algorithm. It should be pointed out that this boundary algorithm is directly making use of the wave values at discrete grid points to extrapolate the boundary values. Because of the nature of the present boundary condition construction, it is not particularly

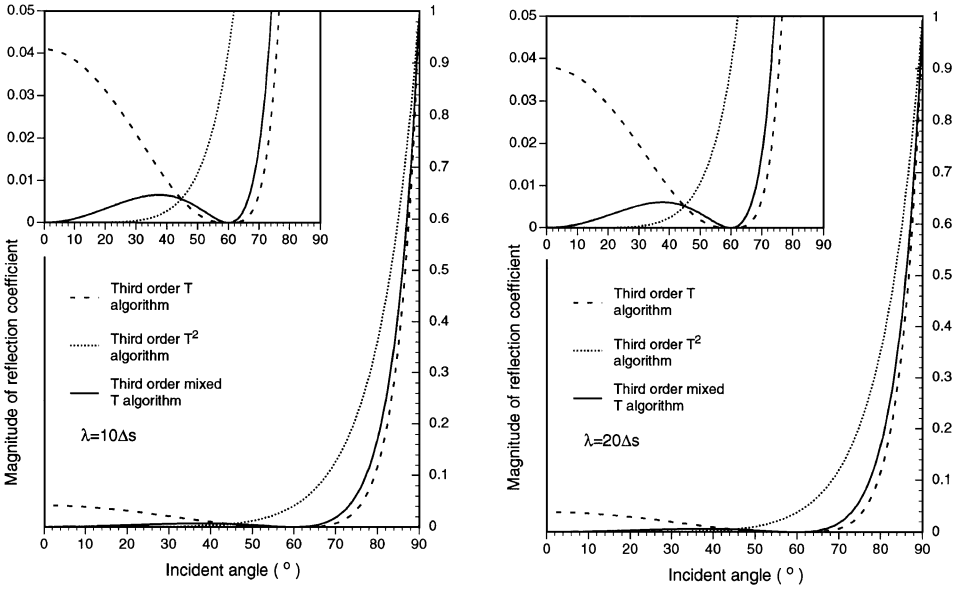

FIG. 2. Comparison of the reflection coefficients associated with the T, T^2, and the mixed T algorithms. The small diagrams are the enlargements of the reflection coefficients for small values.

meaningful to express the boundary equation in a continuous operator form. The reflection coefficient associated with the algorithm given by (2.24) is expressed by

$$R_{MT} = -e^{i2k_x\Delta s I_b - iNk_x\Delta s}\left\{\frac{\sin[k\Delta s(c\Delta t/\Delta s - \cos\alpha)/2]}{\sin[k\Delta s(c\Delta t/\Delta s + \cos\alpha)/2]}\right\}^{N-M} \times \left\{\frac{\sin[k\Delta s(2c\Delta t/\Delta s - \cos\alpha)/2]}{\sin[k\Delta s(2c\Delta t/\Delta s + \cos\alpha)/2]}\right\}^{M}. \quad (2.25)$$

For a third-order algorithm involving $N = 3$ and $M = 1$, the magnitude of the reflection coefficient given by (2.25) is shown in Fig. 2 for comparison with those of the T and T^2 algorithms. The reflection coefficient associated with the mixed T algorithm is less than 1% for the incident angle from 0° to about 70°. It is apparent that the present algorithm has absorbed the advantages of the preceding two algorithms.

For application to the discrete computation, we present the second- and third-order mixed T algorithms in explicit forms. The second-order formula ($N = 2$ and $M = 1$) for the right-side boundary can be expressed by

$$U^{n+1}(I_b, J, K) = U^n(I_b - 1, J, K) + U^{n-1}(I_b - 1, J, K) - U^{n-2}(I_b - 2, J, K), \quad (2.26)$$

while the counterpart of the third order ($N = 3$ amd $M = 1$) is

$$U^{n+1}(I_b, J, K) = 2U^n(I_b - 1, J, K) + U^{n-1}(I_b - 1, J, K) - U^{n-1}(I_b - 2, J, K) - 2U^{n-2}(I_b - 2, J, K) + U^{n-3}(I_b - 3, J, K). \quad (2.27)$$

It should be pointed out that the mixed T algorithm is an economic boundary condition in terms of the required number of variables to be stored for updating the boundary value. Two

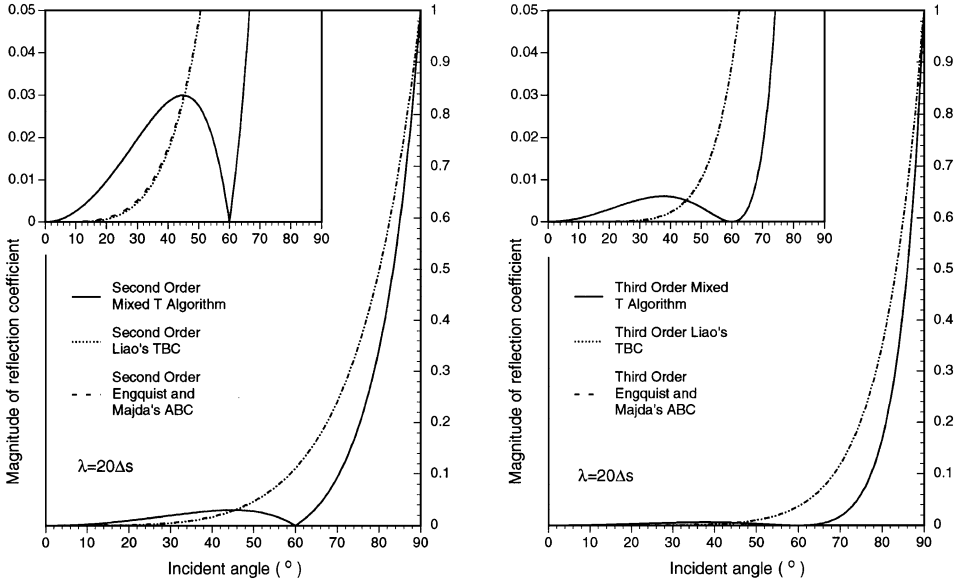

FIG. 3. Same as Fig. 2, except for Liao's TBC, Engquist and Majda's ABC, and the mixed T algorithm.

and six variables are needed for the second- and third-order mixed T algorithms, respectively. The third-order T^2 algorithm, however, requires nine variables, while 14 variables are needed for the third-order Liao's TBC. Furthermore, we also note that the mixed T algorithm is more efficient than Liao's TBC given by (2.2) because the former is less reflectional for a wider range of incident angles. The reflection coefficient of Liao's TBC has been derived by Chew and Wagner [17]. Figure 3 compares the spurious reflection associated with Liao's TBC and the mixed T algorithm. Note that $c\Delta t/\Delta = 0.5$ is used in the calculation for Liao's TBC. It is clear that the reflection feature of Liao's TBC is very similar to that of the T algorithm. Although Liao's TBC is slightly more accurate than the mixed T algorithm for incident angles smaller than 45°, it produces significant reflections for large incident angles. Figure 3 also presents the reflection coefficient for the typical ABC that was derived by Engquist and Majda [19] on the basis of OWWE. Higdon [20] showed that the pth-order boundary condition of Engquist and Majda is equivalent to

$$\left(\frac{\partial}{\partial t} - \frac{\partial}{\partial x}\right)^p U = 0, \tag{2.28}$$

where the boundary is supposed to be at $x = 0$ and the wave speed is scaled to unit. The reflection coefficient associated with the preceding equation is

$$R = -\left(\frac{1-\cos\alpha}{1+\cos\alpha}\right)^p. \tag{2.29}$$

From Fig. 3 it is evident that the reflection coefficient derived from Engquist and Majda's ABC differs only slightly from Liao's TBC.

D. *Stabilize Mixed T Algorithm*

In the preceding discussion, the outgoing wave is assumed to be a plane wave in the vicinity of the boundary locally. Under this assumption amplification of the computed wave values can occur. In fact, if (2.26) and (2.27) are used, the overflow phenomena will eventually occur in numerical computations. Moghaddam and Chew [16] studied the instability associated with Liao's TBC. By applying the Z-transform to Liao's TBC given by (2.2), they found that one root of the characteristic equation of the Z-transform locates on the unit circle around the origin in the complex plane, which can be driven outside the circle due to roundoff errors in numerical computations, rendering the system unstable. To circumvent the instability, they further suggested that adiabatic loss terms be added to $T_{1,1}$, $T_{1,2}$, and $T_{1,3}$ in (2.2). In the present investigation, we find that the instability is essentially associated with the location-dependent amplitude of the outgoing or scattered wave. We have derived a stabilized scheme for the boundary equation.

To understand the instability of the boundary condition, the stability analysis should be carried out for the coupled system of the boundary equation and the finite difference equations applied to the inner grid points, which becomes an eigenvalue problem. However, it appears not possible to solve this eigenvalue problem because the system is extremely complicated. Recently, Min *et al.* [21] stated that the Fourier or Von Neumann method can be employed to investigate the instability of the boundary condition without considering the coupled system. The method is based on the principle that f(t, x, y, z), a general function of time and space, can be represented by its Fourier spectrum as

$$f(t, x, y, z) = \left(\frac{1}{2\pi}\right)^3 \iiint_{-\infty}^{\infty} F(t, k_x, k_y, k_z) e^{i(k_x x + k_y y + k_z z)}\, dx\, dy\, dz, \tag{2.30}$$

where $F(t, k_x, k_y, k_z)$ is the Fourier spectrum of f(t, x, y, z), and k_x, k_y, and k_z are the components of the wave vector. Thus, the stability of the boundary is ensured by the stability of $F(t, k_x, k_y, k_z) \exp[i(k_x x + k_y y + k_z z)]$. Since the plane wave condition is assumed in the proximity of the boundary locally, the stability analysis is only required for a harmonic wave mode which is in the form of $\exp[i(k_x x + k_y y + k_z z) - i\omega t]$. In practice, this procedure assumes that the separation of variables is allowed for the wave value; that is,

$$U^n(I, J, K) = \rho^n e^{i(k_x I + k_y J + k_z K)\Delta s}, \tag{2.31}$$

where ρ is the amplifying coefficient for the one step time-updating iteration. If $|\rho| \leq 1$, the algorithm is stable; otherwise, amplification of the simulated field takes place and the numerical overflow will occur eventually. Substituting (2.31) into the T, T^2, and mixed T boundary equations, we can obtain the value for ρ. For example, for the T algorithm we have

$$\rho = e^{-ik_x \Delta s}, \quad \text{or} \quad |\rho| = 1. \tag{2.32}$$

That is, the amplification in the temporal updating process is neutral and the boundary condition will be stable. However, overflow can always be produced by the T algorithm even if double-precision arithmetic is used. In addition, we find that the higher the order of the algorithm is used, the sooner the overflow will occur. The difference between the theoretical analysis and computational aspect is because the preceding method is valid only

for an unbounded or periodic boundary system; otherwise, the location-dependent of the spectrum, $F(t, k_x, k_y, k_z)$, must be accounted for in the stability analysis.

For simplicity, but without losing of generality, we consider the scattering of a scalar harmonic plane wave by a particle. The wave equation for the scalar wave is given by

$$\frac{1}{c^2}\frac{\partial^2}{\partial t^2}U - \nabla^2 U = 0. \tag{2.33}$$

The Helmholtz equation associated with (2.33) is then

$$\nabla^2 U + k^2 U = 0, \tag{2.34}$$

where $k = \omega/c$ is the wavenumber. It can be proven that the radiation or outgoing solution to (2.34) in the 3D case be expressed by the equation [10]

$$U(R, \theta, \varphi) = \frac{e^{ikR}}{R}\sum_{L=0}^{\infty}\frac{f_L(\theta, \varphi)}{R^L}, \tag{2.35}$$

where θ and φ are the zenith and azimuthal angles, respectively and R is the distance between the observing position to the source. The counterpart of (2.35) in the 2D case can be written as [10]

$$U(R, \varphi) = \sqrt{\frac{2}{\pi kR}}e^{i(kR-\pi/2)}\sum_{L=0}^{\infty}\frac{f_L(\varphi)}{R^L}. \tag{2.36}$$

In the following analysis of the stability, we only consider the 3D case because the same result can be obtained for the 2D case. As shown in Fig. 4, the artificial boundary is located far enough so that only the first term in the expansion on the right-hand side of (2.35) needs to be considered because other terms are insignificant. Thus, we have

$$U(R, \theta, \varphi) \approx A(R)e^{ikR}f_0(\theta, \varphi), \tag{2.37a}$$

$$A(R) = 1/R. \tag{2.37b}$$

Therefore, the location-dependence of the wave amplitude at the grid points $P_1, P_2, P_3, \ldots$ which are along the normal of the boundary face can be expressed by

$$\begin{aligned} A_{p_L} &= \frac{1}{[(x_b - L\Delta s)^2 + y^2 + z^2]^{1/2}} \\ &= \frac{1}{R_b}\left[1 - 2L\Delta s x_b/R_b^2 + (L\Delta s/R_b)^2\right]^{-1/2} \\ &\approx A_b e^{L\Delta s\cos\alpha/R_b} \quad \text{for } L = 1, 2, 3, \ldots, \end{aligned} \tag{2.38}$$

where $A_b = 1/Rb$ in which $R_b = (x_b^2 + y^2 + z^2)^{1/2}$ is the distance between the source and the boundary point. In the derivation of (2.38), $(L\Delta s/R_b)^2$ is ignored because it is much smallar than $2x_bL\Delta s/R_b^2$ and $\Delta s/R_b \ll 1$ is also assumed. Let $\gamma = \Delta s\cos\alpha/R_b$; then the amplitude of the harmonic wave in the proximity of the boundary is

$$A_{P_L} = A_b e^{\gamma L}, \quad L = 1, 2, 3, \ldots. \tag{2.39}$$

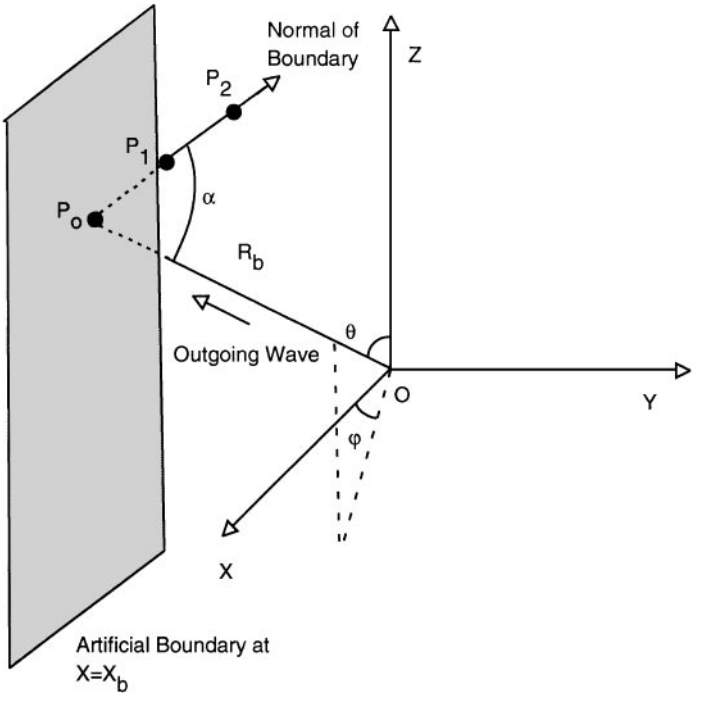

FIG. 4. Geometry for studying the numerical instability associated with the transmitting boundary condition.

Thus, if the variation of the amplitude is accounted for, then (2.31) should be

$$U^n(I, J, K) = \rho^n e^{\gamma(I_b - I)} e^{i(k_x I + k_y J + k_z K)\Delta s}. \tag{2.40}$$

Substituting (2.40) into the T algorithm, we obtain

$$\rho = e^{\gamma} e^{-ik_x \Delta s}, \quad \text{or} \quad |\rho| = e^{\gamma} > 1. \tag{2.41}$$

That is, the simulated field will undergo an amplification, leading to numerical instability. Physically, the instability occurs because the wave amplitude is assumed to be independent of the spatial location near the boundary in the derivation of the boundary equations presented in Subsections 2A and 2B. When the wave value at an interior point that is $L\Delta s$ away from the boundary is extrapolated to obtain the boundary value, an amplification given by a factor of $\exp(\gamma L)$ is implied. For the Nth-order algorithm, $e^{N\gamma}$ is implied, in conjunction with the wave value at the most inner grid point along the normal of the boundary. Therefore, the higher order algorithm will lead to serious amplification.

In order to obtain a stable algorithm, we introduce spatial diffusive coefficients in the boundary equation to suppress the preceding amplification. Consider a boundary point at (I_b, J, K). If an interior point at $(I_b - L, J, K)$ is involved in the extrapolation of the boundary value, the corresponding coefficient is $\exp(\gamma L)$. To circumvent the amplification, the diffusive coefficient should be $\exp(-\gamma L)$. Thus, the stabilized schemes associated with (2.26) and (2.27) can be rewritten as

$$U^{n+1}(I_b, J, K) = e^{-\gamma}[U^n(I_b - 1, J, K) + U^{n-1}(I_b - 1, J, K)] - e^{-2\gamma} U^{n-2}(I_b - 2, J, K), \tag{2.42}$$

and

$$U^{n+1}(I_b, J, K) = e^{-\gamma}[2U^n(I_b - 1, J, K) + U^{n-1}(I_b - 1, J, K)] - e^{-2\gamma}[U^{n-1}(I_b - 2, J, K) + 2U^{n-2}(I_b - 2, J, K)] + e^{-3\gamma}U^{n-3}(I_b - 3, J, K). \quad (2.43)$$

In practice, the value of γ is unknown and must be determined empirically. In this investigation, by using the trial and error method, we find that $\gamma = 0.05$ and 0.01–0.005 are appropriate for a continuous sinusoidal wave source and a pulse source, respectively. The boundary equations given by (2.42) and (2.43) are extremely stable in numerical computations. For a 2D small grid with the size of 61×31, we have run the FDTD code in single-precision arithmetic with a point sinusoidal source. We find that overflow does not occur even for more than 10^5 steps in the time-updating iteration.

3. APPLICABILITY OF THE MIXED T ALGORITHM

In this section, three kinds of numerical experiments are carried out to test the accuracy and stability of the preceding stabilized mixed T algorithm. The accuracy of the present boundary condition is compared with that of the most popular Mur's ABC. First, the Mur's ABC is briefly recapitulated. For simplicity, we only consider the 2D case. The wave equation can be expressed in an operator form as [12]

$$L_x^+ L_x^- U = 0, \quad (3.1)$$

where L_x^+ and L_x^- are OWWE operators given by

$$L_x^+ = D_x + \frac{D_t}{c}\sqrt{1 - c^2 D_y^2/D_x^2}, \quad (3.2a)$$

$$L_x^- = D_x - \frac{D_t}{c}\sqrt{1 - c^2 D_y^2/D_x^2}, \quad (3.2b)$$

in which D_x, D_y, and D_t stand for $\partial/\partial x$, $\partial/\partial y$, and$\partial/\partial t$, respectively. For a boundary, say, the right-side boundary at $x = x_b$, it has been proven that it is completely reflectionless if in the following OWWE is satisfied [14, 13]:

$$L_x^+ U\big|_{x=x_b} = 0. \quad (3.3)$$

The OWWE operator L_x^+, however, is a pseudo-differential operator due to the existence of the radical. Thus, (3.3) cannot be discretized as a finite difference equation. In order to obtain the discrete form for OWWE, various rational functions can be used to approximate the OWWE operator. The most common approach is the expansion of the radical using the Taylor series, as presented by Engquist and Majda [19] and Mur [14]. Keeping the first term and the first two terms in the Taylor expansion will lead to the first- and second-order Mur's ABC, respectively. In practice, ABC is discretized by using the central-difference scheme for the differentials in time and space. The reflection coefficient associated with Mur's ABC has been obtained by Ray [22]. Figure 5 compares the reflection coefficient for Mur's ABC and the mixed T algorithm. It is evident that the mixed T algorithm appears to function better and it is not sensitive to the wavelength of incident waves.

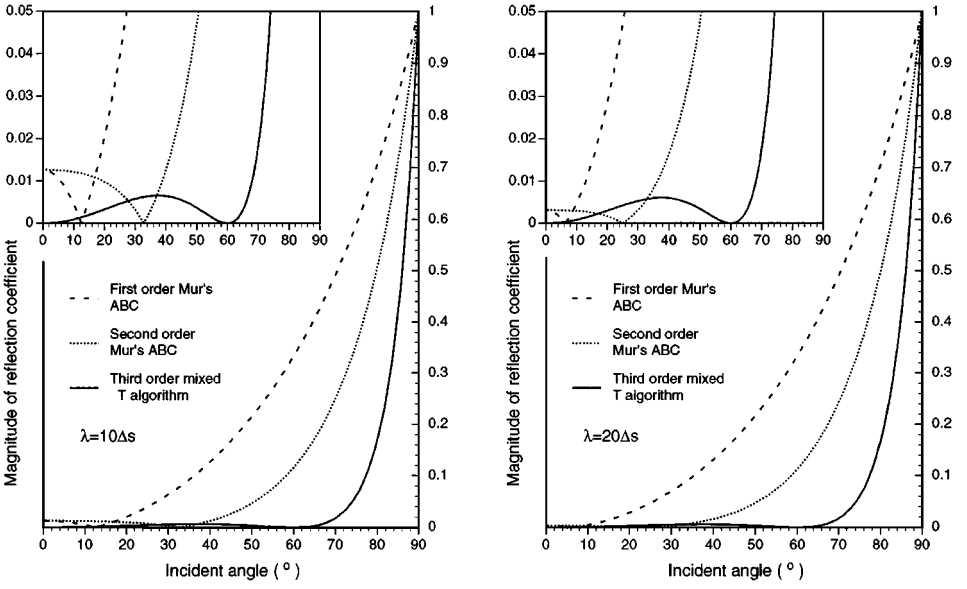

FIG. 5. Same as Fig. 2, except for Mur's ABC and the mixed T algorithm.

A. *Experiment 1*

In this experiment, we consider the propagation of a TM wave which is excited by a sinusoidal point source. The governing equations for the electromagnetic fields are

$$\frac{1}{c}\frac{\partial E_z}{\partial t} = \frac{\partial H_y}{\partial x} - \frac{\partial H_x}{\partial y} + A\lambda \sin\left(\frac{2\pi}{\lambda}ct\right)h(t)\delta(\vec{r} - \vec{r}_o), \tag{3.4a}$$

$$\frac{1}{c}\frac{\partial H_x}{\partial t} = -\frac{\partial E_z}{\partial y}, \tag{3.4b}$$

$$\frac{1}{c}\frac{\partial H_y}{\partial t} = \frac{\partial E_z}{\partial x}, \tag{3.4c}$$

where h(t) is the Heaviside unit-step function, and $\delta(\vec{r} - \vec{r}_o)$ is the Dirac-δ function. In numerical computations, we have selected $A = 10$ and $\lambda = 20\Delta s$. The finite difference equations associated with (3.4) are given by

$$\begin{aligned} E_z^{n+1}(I, J) = EZ_z^n(I, J) + \frac{c\Delta t}{\Delta s}\Big\{&\left[H_y^{n+1/2}(I + 1/2, J) - H_y^{n+1/2}(I - 1/2, J)\right] \\ &- \left[H_x^{n+1/2}(I, J + 1/2) - H_x^{n+1/2}(I, J - 1/2)\right]\Big\} \\ &+ A\frac{c\Delta t}{\Delta s^2}\lambda \sin\left[\frac{2\pi}{\lambda}c(n + 1/2)\Delta t\right]h(n + 1/2)\delta_{I,I_o}\delta_{J,J_o}, \end{aligned} \tag{3.5a}$$

$$H_x^{n+1/2}(I, J + 1/2) = H_x^{n-1/2}(I, J + 1/2) - \frac{c\Delta t}{\Delta s}\left[E_z^n(I, J + 1) - E_z^n(I, J)\right], \tag{3.5b}$$

$$H_y^{n+1/2}(I + 1/2, J) = H_y^{n-1/2}(I + 1/2, J) + \frac{c\Delta t}{\Delta s}\left[E_z^n(I + 1, J) - E_z^n(I, J)\right], \tag{3.5c}$$

where δ_{I,I_o} and δ_{J,J_o} are the Kronecker symbols and (I_o, J_o) is the location of the source. The simulation of the TM wave propagation is restricted to a 61×31 grid mesh using Mur's

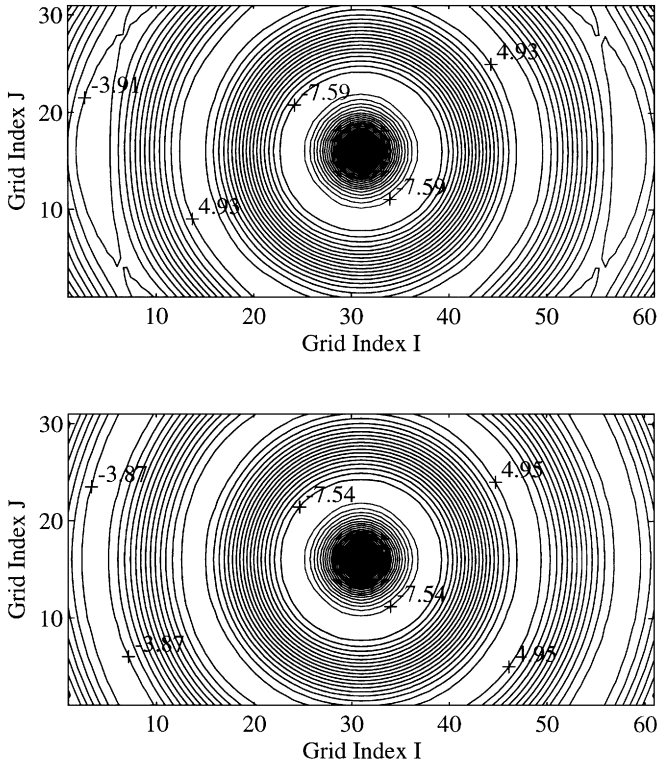

FIG. 6. Snapshots of the electric field at the time step n = 1200. A sinusoidal source is located at (I, J) = (31, 16). The upper diagram is the result produced by Mur's ABC, while the lower diagram is the result obtained from the mixed T algorithm.

ABC or the mixed T transmitting boundary condition. It is known that the contours of the electromagnetic field would be a set of circles centered at the source if the boundary is completely reflectionless. Figure 6 is the snapshot of the electric field at n = 1200 for the case when the source is located at the center of the grid. It is clear that the contours of the electric field are distorted near the left and right boundaries when Mur's ABC is used. The contours are almost perfect circles when the mixed T algorithm is used. Figure 7 is the case when the point source has been moved closer to the lower right corner of the grid. In this case the distortion of the contours is seen for both boundary conditions. However, the distortion is much reduced by using the mixed T algorithm. Next, the wave equation for the electric field can be obtained from (3.4) as

$$\frac{\partial^2 E_z}{\partial x^2} + \frac{\partial^2 E_z}{\partial y^2} + \frac{\partial^2 E_z}{\partial z^2} - \frac{1}{c^2}\frac{\partial^2 E_z}{\partial t^2} = -2\pi A \cos\left(\frac{2\pi}{\lambda} ct\right) h(t)\delta(\vec{r} - \vec{r}_o). \qquad (3.6)$$

Following Achenbech [23], the exact solution for (3.6) is given by

$$E_Z(\vec{r}, t) = Ac \int_o^{t-R/c} \frac{\cos(2\pi c\tau/\lambda)}{[c^2(t-\tau)^2 - R^2]^{1/2}} d\tau \quad \text{for } t - R/c \geq 0, \qquad (3.7)$$

where $R = |\vec{r} - \vec{r}_0|$ in which $\vec{r}_o$ is the position of the source. It should be noted that the

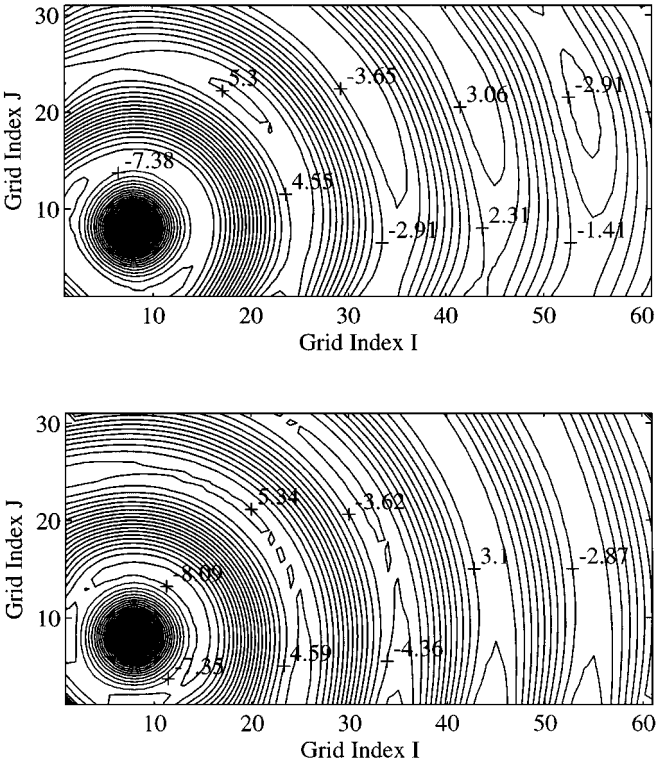

FIG. 7. Same as Fig. 6, except that the source is located at (I, J) = (8, 8).

exact solution given by Mur [14] is not correct because the upper limit of the integration in his equation (20) should not be infinite. Figures 8 and 9 show the comparison between the FDTD results and the exact solution. In Fig. 8 the electric field is seen along the lines parallel to the x-axis and through the source. Both Mur's ABC and the mixed T algorithm perform well, if the source is located at the center of the grid, although slight computational errors associated with Mur's ABC are still detectable in the proximity of the boundary. When the source is located at the grid point (8, 8), significant errors can be observed due to the reflection of Mur's ABC. Figure 9 is the electric field observed along the lines through the source and parallel to the y-axis. Again, the mixed T algorithm performs more accurately than Mur's ABC.

B. *Experiment 2*

An objective method to test the spurious reflection of a boundary condition is to simultaneously simulate the wave propagation in small and large domains which share the same origin or center. This method has been widely used by other researchers [12, 13]. As shown in Fig.10, the small domain is the test domain within which the performance of its boundary will be tested. The large domain should be big enough so that the reflection from the outer boundary will not enter the small domain by the time the numerical experiment is terminated. The experiment is carried out with respect to the electric field. The field is observed within the overlapped part of the two domains. Let the fields associated with the

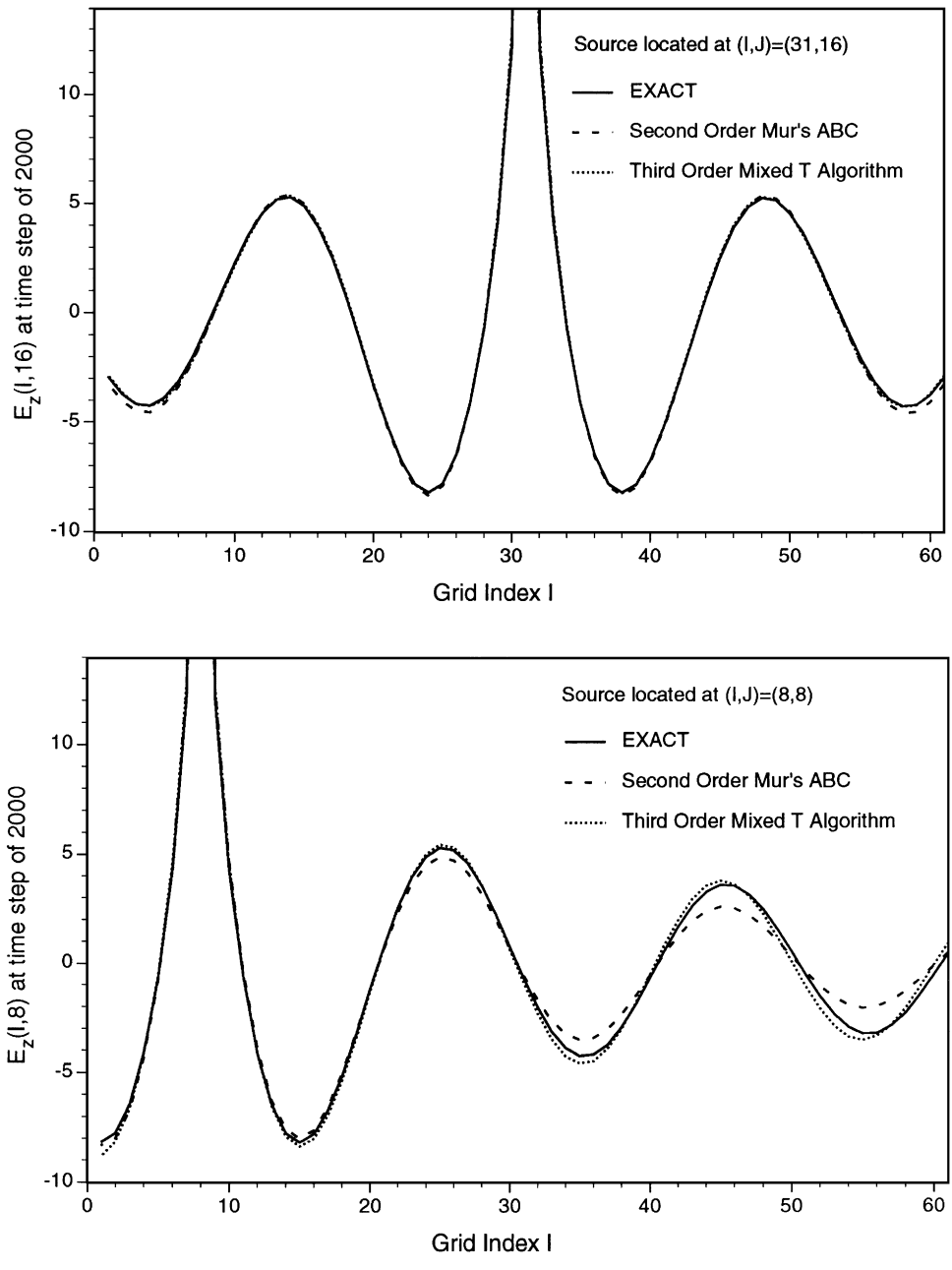

FIG. 8. Comparison of the electric field obtained by the FDTD method and the exact solution. The observation of the fields is along the lines parallel the X-axis and through the source.

small and large domains be $E_z^n(I, J)$ and $\tilde{E}_z^n(I, J)$, respectively. Since the reflection from the outer boundary has not reached the overlapped region $\tilde{E}_z^n$ (I, J) within the overlapped domain is reflection-free. Then, for the reflected wave we have

$$D^n(I, J) = E_z^n(I, J) - \tilde{E}_z^n(I, J). \tag{3.8}$$

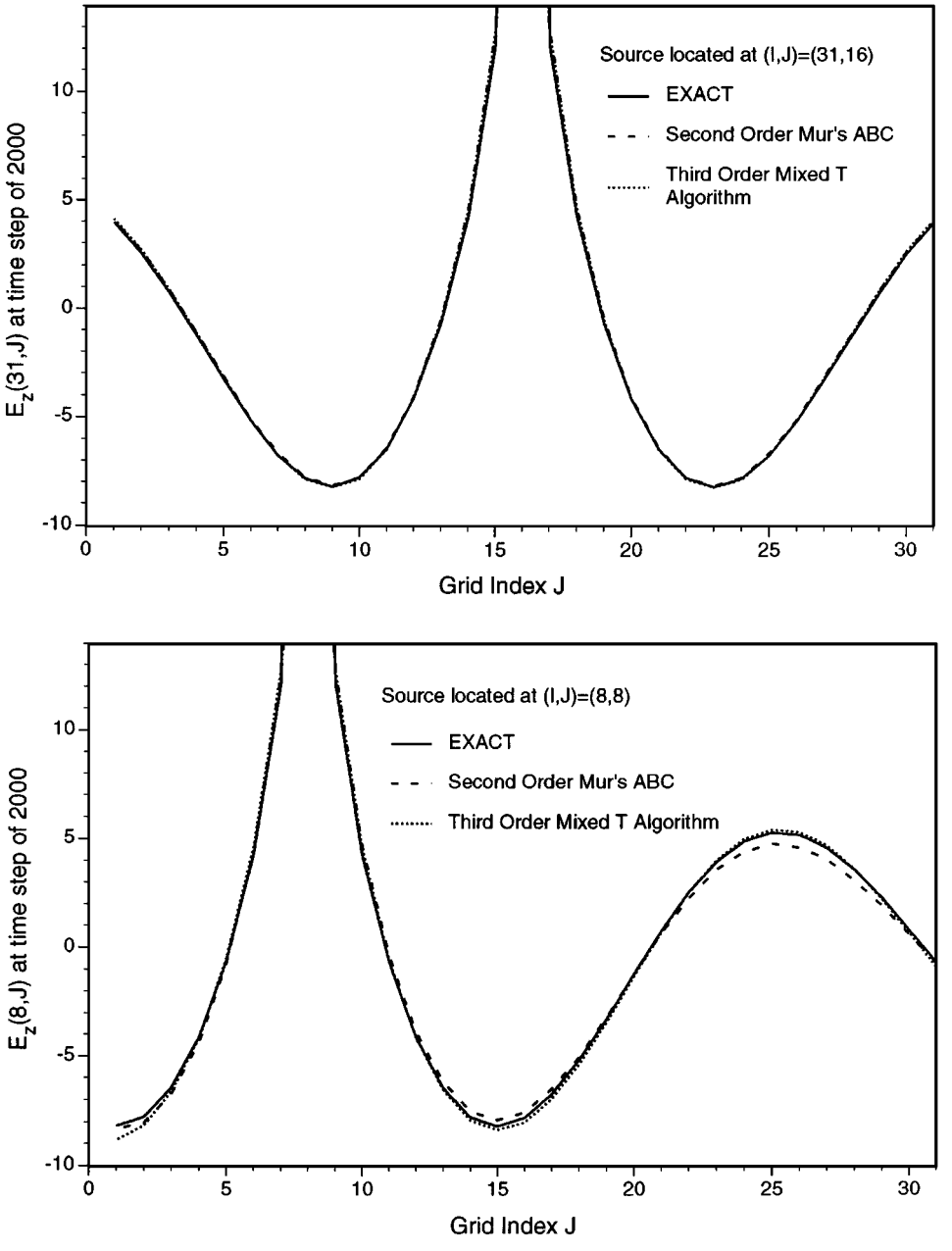

FIG. 9. Same as Fig. 8, except that the observation is performed along the lines parallel to the Y-axis and through the source.

Further, we can define the global measure of the spurious reflection as

$$D = \sum_I \sum_J [D^n(I, J)]^2$$

$$= \sum_I \sum_J \left[E_z^n(I, J) - \tilde{E}_z^n(I, J)\right]^2, \tag{3.9}$$

where the summation is performed over the grid points inside the overlapped domain.

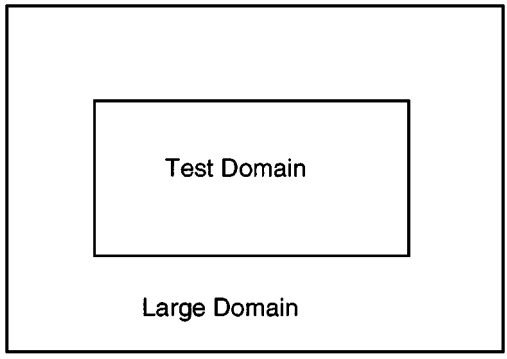

FIG. 10. Small and large domains used for testing the reflection of an artificial boundary.

In this experiment a pulse point source located at the center of the domain is used. The test domain is the size of 101×51, and a "white space" consisting of 30 grid points is used for the distance between the inner and outer boundaries. The time-marching iteration should be terminated at time step $n = 170$; otherwise, the reflection from the outer boundary will center the overlapped region at this moment. The following extremely smooth compact pulse presented by Kriegsmann *et al.* [24] is used in this experiment:

$$\text{source} = \begin{cases} \frac{1}{320}\left[10 - 15\cos\left(\frac{n\pi}{20}\right) + 6\cos\left(\frac{n\pi}{10}\right) - \cos\left(\frac{3n\pi}{20}\right)\right] & \text{for } n \le 40 \\ 0 & \text{for } n > 40. \end{cases} \tag{3.10}$$

The snapshot of the reflected electric field at $n = 100$ along $J = 2$ is shown in Fig. 11, where the global measure of the reflection error is also shown. The results show a phase difference of about π. The magnitude of the reflection introduced by Mur's ABC is much larger than that by the mixed T algorithm. Moreover, from the global reflection measure, it is known that the maximum global error occurs when the peak of the pulse has passed the narrow sides of the inner boundary. The maximum error produced by Mur's ABC is about 3 times larger than that by the mixed T algorithm. This numerical experiment also indicates that the mixed T algorithm is more accurate.

C. *Experiment 3*

In the two preceding experiments, the source of the outgoing wave is just a point source. For the scattering of light by an object, the source of the outgoing wave, however, has a finite extension. Due to the scattering by various parts of the object, a number of waves may arrive at the boundary simultaneously. To test the applicability of the mixed T algorithm to this condition, the scattering of a TM wave by an infinite circular cylinder is solved by the FDTD method since the exact solution is available for comparison. The procedure concerning the application of the FDTD technique to the scattering by the polarized wave in the 2D case has been presented in our previous study [16]. First, a Gaussian pule is used as the incident wave, and the scattering process is simulated explicitly by updating the discretized Maxwell equations within the truncated domain. The harmonic wave mode of interest is then determined by performing the Fourier transform to the computed field which is time-dependent. Subsequently, the near-field so obtained is transformed to far-field on the basis of equivalent electric and magnetic currents. The scattered TM wave in the far-field

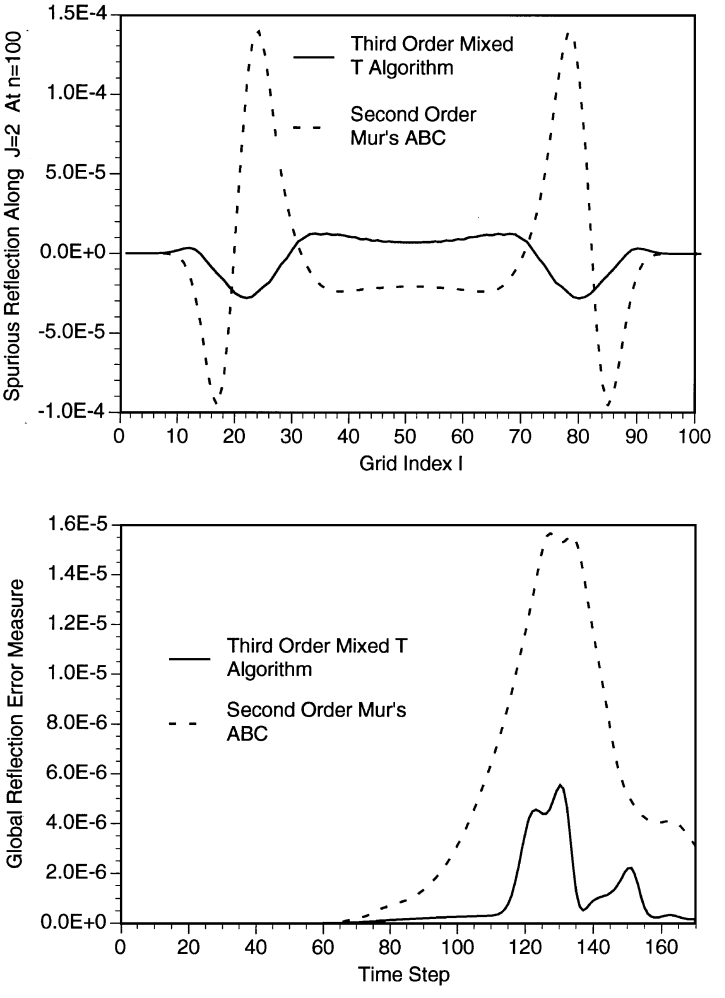

FIG. 11. Spurious reflections of the mixed and Mur's boundary conditions for a pulse source.

can be expressed by

$$E_z^s(r, \varphi) = \left(\frac{2}{\pi k}\right)^{1/2} e^{i(kr+3\pi/4)-ikx} F(\varphi) E_z^i, \tag{3.11}$$

where φ is the scattering angle, r is the distance from the particle to the observing point, and the scattering function $F(\varphi)$ is determined by the electromagnetic properties of the particle. From (3.11), the normalized scattering phase function can be defined by

$$P(\varphi) = \frac{2}{k\pi} \frac{1}{\sigma_s} |F(\varphi)|^2, \tag{3.12}$$

where σ_s is the scattering cross section of the particle. For a nonabsorptive particle, σ_s is given by

$$\sigma_s = \frac{4}{k} \mathrm{Re}[F(0^\circ)]. \tag{3.13}$$

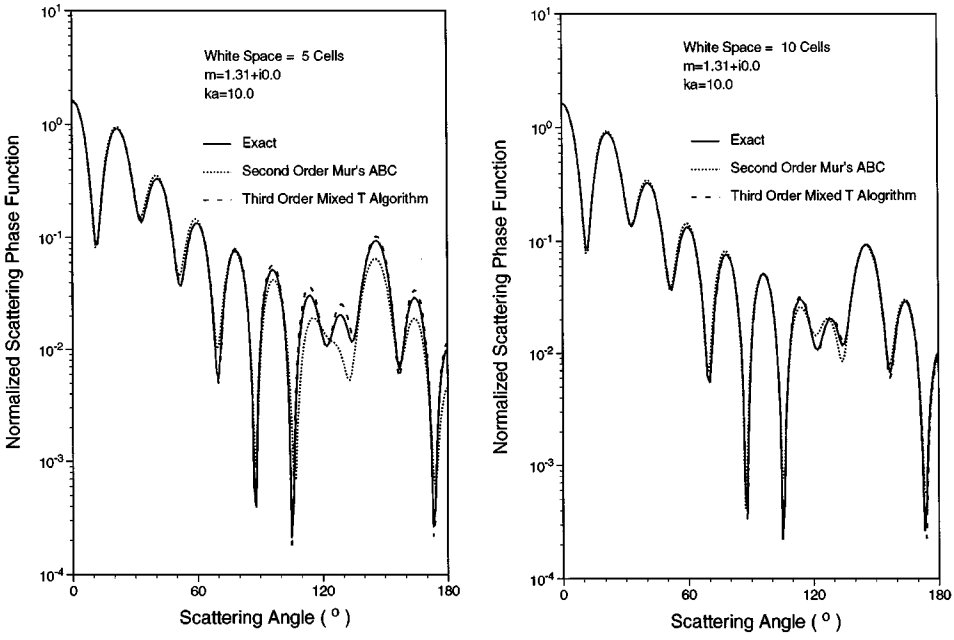

FIG. 12. Normalized scattering phase functions of an infinite circular cylinder computed by the FDTD and exact methods.

Figure 12 shows that the normalized phase function is obtained by the FDTD technique and the exact method. It can be seen that significant errors are produced for the scattering angles around 120° if Mur's ABC is used along with a "white space" of five cells. The accuracy of the FDTD solution is significantly improved by using the mixed T algorithm with the same "white space," although slight deviations are still detectable for large scattering angles. When the "white space" is increased to 10 cells, the results obtained by using the mixed T algorithm almost converges to the exact solution, whereas Mur's ABC still produces significant errors around the scattering angle of 120°. Clearly, Mur's ABC requires more "white space" between the boundary and the scattering object to converge the scattering solution.

Figure 13 displays the scattering efficiency, the ratio of the scattering cross-section area to the projection cross-section area of the particle. Excellent performance is shown for both Mur's ABC and the mixed T algorithm when the size parameter is less than 11. However, for larger size parameters the results obtained from the mixed T algorithm are more accurate. It should noted that the errors in the case of large size parameters are partly caused by the staircasing approximation in defining the particle shape in a Cartesian grid, and they are also caused by the finite difference approximation in discretizing the differential equations. Since the pulse technique is used in the computation, the wavelength concerned in the Fourier transform is shorter for large size parameters than for small size parameters. For a longer wavelength, not only is the staircasing effect small, but also does the numerical dispersion associated with finite difference approximation decrease.

4. CONCLUSIONS

We have developed a mixed T algorithm to truncate the spatial domain in modeling light scattering processes by using the finite-difference technique. Our algorithm is a

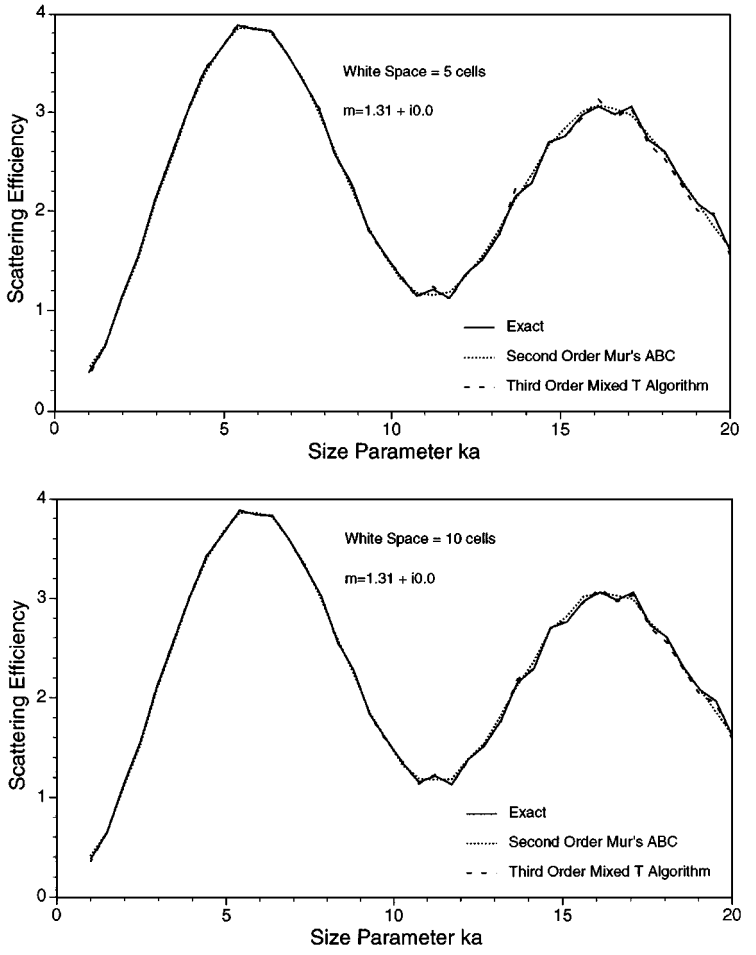

FIG. 13. Scattering efficiencies involving infinite circular cylinders computed by the FDTD and exact methods.

generalization of the transmitting boundary condition developed by Liao *et al*. [15]. The improved boundary condition in this algorithm is numerically economic and produces more accurate results for large incident angles. The applicability of the mixed T algorithm has been verified by three numerical experiments. These include the propagation of a TM wave excited by a sinusoidal point source, simultaneous simulation of the wave propagation in small and large domains that share the same origin, and the scattering of a TM wave by an infinite circular cylinder. It is shown that the accuracy of the boundary condition proposed in this study is improved, in comparison with the popular absorbing boundary condition developed by Mur [14]. We find that a "white space" of 10 cells is sufficiently enough for applications to the scattering of light by a dielectric object if the mixed T algorithm is used. We have successfully applied this algorithm to the solution of light scattering by nonspherical particles with defined and irregular shapes and compositions.

ACKNOWLEDGMENTS

This research was supported by NSF Grant ATM-93-1521, NASA Grants NAG1-1719, NAG5-2678, and DOE Grant DE-FG03-95ER61991. Some of the computational results presented in this paper were obtained using CRAY Y-MP 8/864 supercomputer at the National Center for Atmospheric Research, sponsored by NSF.

REFERENCES

1. K. N. Liou, *Introduction to Atmospheric Radiation* (Academic Press, New York, 1980), p. 392.
2. K. N. Liou, *Radiation and Cloud Processes in the Atmosphere* (Oxford Univ. Press, New York, 1992), p. 487.
3. Y. Takano and K. N. Liou, Solar radiation transfer in cirrus clouds. Part I. Single scattering and optical properties of hexagonal ice crystals, *J. Atmos. Sci.* **46**, 3 (1989).
4. K. S. Yee, Numerical solution of initial boundary value problems involving Maxwell's equations in isotropic media, *IEEE Trans. Antennas Propagat.* **Ap-14**, 302 (1966).
5. A. Taflove and M. E. Brodwin, Numerical solution of steady-state electromagnetic scattering problem using the time-dependent Maxwell's equation, *IEEE Trans. Microwave Theory Tech.* **MTT-23**, 623 (1975).
6. K. Umashankar and A. Taflove, A novel method to analyze electromagnetic scattering of complex objects, *IEEE Trans. Electromagn. Compat.* **EMC-24**, 397 (1982).
7. C. M. Furse, S. P. Mathur, and O. P. Gandi, Improvements to the finite-difference time-domain method for calculating the radar cross section of a perfectly conducting target, *IEEE Trans. Microwave Theory Tech.* **38**, 919 (1990).
8. A. Sommerfeld, *Partial Differential Equations* (Academic Press, New York, 1949), p. 333.
9. A. C. Vastano and R. O. Reid, Tsunami Response for Islands: Verification of a numerical procedure, *J. Marine Res.* **25**, 129 (1967).
10. A. Bayliss and E. Turkel, Radiation boundary conditions for wave-like equations, *Commun. Pure Appl. Math.* **33**, 707 (1980).
11. C. Britt, Solution of electromagnetic scattering problems using time domain techniques, *IEEE Trans. Antennas Propagat.* **37**, 1181 (1989).
12. T. Moore, J. G. Blaschak, A. Taflove, and G. A. Kriegsmann, Theory and application of radiation boundary operators, *IEEE Trans. Antennas Propagat.* **36**, 1797 (1988).
13. J. Blaschak and G. A. Kriegsmann, A comparative study of absorbing boundary conditions, *J. Comput. Phys.* **77**, 109 (1988).
14. G. Mur, Absorbing boundary conditions for the finite-difference approximation of the time-domain electromagnetic-field equations, *IEEE Trans. Electromagn. Compat.* **EMC-23**, 377 (1981).
15. Z. Liao, H. L. Wong, B. Yang, and Y. Yuan, A transmitting boundary for transient wave analyses, *Sci. Sinica Ser. A* **27**, 1063 (1984).
16. M. Moghaddam and W. C. Chew, Stabilizing Liao's absorbing boundary conditions using single-precision arithmetic, *IEEE AP-S Int. Sympos. Digest*, 430 (1991).
17. W. C. Chew and R. L. Wagner, A modified form of Liao's absorbing boundary condition, *IEEE AP-S Int. Sympos. Digest*, 536 (1992).
18. P. Yang and K. N. Liou, Light scattering by hexagonal ice crystals: Comparison of FDTD and geometric optics models, *J. Opt. Soc. Amer. A* **12**, 162 (1995).
19. B. Engquist and A. Majda, Absorbing boundary conditions for the numerical simulation of waves, *Math. Comp.* **31**, 629 (1997).
20. R. L. Higdon, Absorbing boundary conditions for difference approximations to multidimensional wave equation, *Math. Comp.* **47**, 437 (1986).
21. X. Min, W. Sun, and K. M. Chen, Stability analysis of the finite-time domain method applied to unbounded electromagnetic problems, *IEEE AP-S Int. Sympos. Digest*, 1640 (1990).
22. S. L. Ray, Characterization of radiation boundary conditions used in the finite-difference time-domain method, *AP-S Int. Sympos. Digest*, 30 (1989).
23. J. D. Achenbach, *Wave Propagation in Elastic solids* (North-Holland, Amsterdam, 1973), Chap. 3.
24. G. A. Kriegsmann, A. N. Norris, and E. L. Reiss, Acoustic pulse scattering by baffled membranes, *J. Acoust. Soc. Amer.* **79**, 1 (1986).